

Tuning magnetization compensation and Curie temperatures in epitaxial rare earth iron garnet filmsTemuujin Bayaraa ¹, Changsong Xu,^{1,2,*} Davis Campbell,¹ and L. Bellaiche^{1,2}¹*Physics Department, University of Arkansas, Fayetteville, Arkansas 72701, United States*²*Institute for Nanoscience and Engineering, University of Arkansas, Fayetteville, Arkansas 72701, United States*

(Received 26 July 2019; revised manuscript received 17 November 2019; published 12 December 2019)

An *ab initio* effective Hamiltonian is developed and used to reveal the effect of misfit strain on magnetic properties of epitaxial (001) films made of a prototypical rare earth iron garnet: Gadolinium iron garnet. It is found that both the magnetization compensation temperature (T_M) and the Curie temperature (T_C) can be significantly and linearly enhanced when varying the strain from tensile to compressive values. Consequently, T_M can be designed to coincide with room temperature, and the magnitude of the magnetization can be optimized at around 300 K when choosing the appropriate substrate. The microscopic origins of these technologically promising effects are further revealed.

DOI: [10.1103/PhysRevB.100.214412](https://doi.org/10.1103/PhysRevB.100.214412)**I. INTRODUCTION**

Insulating magnetic garnets have been a subject of interest in the past decades due to their promise towards spin switching, magneto-optical switching, spintronics, and other spin-based applications [1–4]. Moreover, as ferrimagnetic insulators, rare earth iron garnets $\text{Re}_3\text{Fe}_5\text{O}$ (RIG) have been extensively studied, due to their complex magnetic structure, high Curie temperature ($T_C > 500$ K), relatively large band gap (~ 2.8 eV) and chemical stability [4–15]. More precisely, RIGs adopt a ferrimagnetic ordering, which originates from (i) the strong antiferromagnetic coupling between an inequivalent number of Fe ions that occupy the tetrahedral and octahedral sites in a unit cell, and (ii) rare earth ions that sit at the dodecahedral sites with a finite magnetic moment that has been reported to be coupled antiferromagnetically with the tetrahedral Fe moment [11,16]. Moreover, the temperature dependence of Re sublattice is more sensitive than the sublattice of Fe, thus as temperature decreases the magnetization of the Re sublattice increases greatly and can lead to the appearance of the so-called compensation temperature (T_M) in some RIGs, where the net magnetization vanishes [7,9,11]. Compensation of magnetization has recently gained interest due to its possible applications in information storage, thermomagnetic switching and laser induced switching [11,17–19]. Tuning this compensation temperature is highly desired for these applications, especially if one succeeds in bringing T_M to room temperature (i.e., around 300 K). In fact, T_M of terbium iron garnet has been reported to change from 248.6 to 335 K when going from bulk to (111) films grown on the gadolinium gallium garnet (GGG) substrate (which induces a compressive strain of 0.5% on the terbium iron garnet films). Such impressive enhancement is believed to be caused by an extrinsic effect, namely the octahedral sites being occupied by a mixture of Fe^{3+} and Tb^{4+} ions in the films [5]. Similarly, the deviation from perfect stoichiometry (which is an extrinsic effect) was reported to affect strain-induced changes of the

compensation temperature of RIG films in the 1960s and 1970s [14,15].

One may wonder if also this compensation temperature (and Curie temperature, T_C , too, if possible) of rare earth iron garnets films can be *significantly and intrinsically* tuned by the misfit strain arising from the substrate, similar to the known strain-induced modification of the paraelectric-to-ferroelectric transition in perovskite oxides (see Refs. [20] and references therein). Understanding the origins of such hypothetical tunings, including what kind of magnetic moments (among those of the rare earth ions and two types of Fe ions) are mostly responsible for them, is also of obvious fundamental interest.

The goal of this article is to take advantage of a presently developed effective Hamiltonian, with all its coefficients being extracted from first-principles technique, and to reveal and explain why misfit strain can indeed drastically and intrinsically affect T_M and T_C in RIG systems. Such dependency can, e.g., render the compensation temperature of gadolinium iron garnet (GIG) films to coincide with room temperature when grown on an appropriate substrate. This paper is organized as follows. Section II provides a description of the computational methods used here. Section III reports and discusses results for the bulk case, as well as the predicted changes in T_M and T_C due to epitaxial strain. Finally, a summary is given in Sec. IV.

II. METHODS

We studied both bulk and epitaxial (001) films made of GIG as a function of temperature and misfit strain. GIG has been chosen because it has the highest T_M among all RIGs at 286 K [9] and is thus already close to room temperature. Here, (001) GIG films are studied for epitaxial strain ranging from -3% (compressive strain) to $+3\%$ (tensile strain), which are realistic [4]. Technically, we use periodic boundary conditions along any direction, including the out-of-plane one. Consequently, we model the sole effect of epitaxial strain on magnetic properties of (001) GIG films (which can help to better understand epitaxial films [20–22]), and our results

*cx002@uark.edu

should be applicable to RIG films that are neither not too thin (to avoid surface effect) nor too thick (that is, the thickness should be below the critical thickness above which structural relaxation of the in-plane lattice vectors begins to occur). Note that such latter critical thickness has been reported to be a couple of nanometers in some RIG films [4,23].

The magnetic interactions of our GIG systems are described by the following effective magnetic Hamiltonian, H :

$$H = H_1^{\text{ex}} + H_2^{\text{ex}}; \text{ with } H_1^{\text{ex}} = \frac{1}{2} \sum_{\langle i,j \rangle_1} J_{1,ij} S_i \cdot S_j$$

and $H_2^{\text{ex}} = \frac{1}{2} \sum_{\langle i,j \rangle_2} J_{2,ij} S_i \cdot S_j,$ (1)

where H_1^{ex} and H_2^{ex} denote the first and second nearest-neighbor (2NN) exchange couplings between different types of ions (these interactions will be described in Table II later on). $S = 5/2$ and $S = 7/2$ are used for Fe and Gd ions, respectively. The J parameters, which characterize the magnetic exchange couplings, are extracted by performing the density functional calculations (DFT) detailed below. Once these parameters are known for the bulk case and each investigated epitaxial strain, Eq. (1) is then employed in parallel tempering Monte Carlo (MC) simulations on $4 \times 4 \times 4$ supercells (each unit cell contains 160 atoms, which implies that our supercell has 10,260 ions, including 4096 magnetic ones) using the heat bath algorithm [24], in order to predict magnetic properties such as the compensation and Curie temperatures. Technically, 2,000 exchange steps are performed in each MC simulation with each exchange step containing 200 sweeps [24].

DFT calculations are carried out via the Vienna *ab initio* simulation package [25] using the projector augmented-wave potentials [26]. The following electrons are treated as valence states for each ion: O $2s$ and $2p$, Fe $3d$, and $4s$, and Gd $5p$, $5d$, and $6s$. The generalized gradient approximation, together with the revised Perdew-Burke-Ernzerhof exchange-correlation functional for solids [27] is employed with an effective Hubbard U parameter of 4 eV for the localized $3d$ electrons of Fe ions and $U = 4$ eV for the localized $4f$ electrons of Gd ions. Such choices were reported to yield accurate results [8,19,28,29]. Since the lowest energy collinear spin configuration has tetrahedron Fe ions arranged antiferromagnetically with respect to the other two sublattices (octahedron Fe and Gd ions) in bulk GIG [8], we adopt such magnetic configuration for bulk and epitaxial films. For any chosen epitaxial strain for the (001) films, the in-plane lattice vectors are frozen in our calculations with their length being related to the misfit strain. All the other structural degrees of freedom of these films, which are the out-of-plane lattice vector and atomic positions, are allowed to relax. In contrast, *all* structural degrees of freedom are allowed to relax in the bulk case. Furthermore, the energy cutoff of 500 eV is used, and the Monkhorst-Pack k -point mesh is chosen to be $2 \times 2 \times 2$ for the 160-atom cubic unit cell. Spin-orbit couplings and noncollinear magnetism are not considered in our calculations since, as we will see below, collinear magnetism can already well reproduce Curie and compensation temperatures in GIG. Additionally, we numerically checked the effect of single ion anisotropy of all three magnetic sites on properties. We did not find any change in T_M and T_C when single ion anisotropies were included. Structural relaxations are performed until the

TABLE I. Atomic positions in the GIG unit cell for bulk GIG and (001) GIG films under a -1% compressive strain.

		Wyckoff position	x	y	z
Bulk case	O	96h	0.972	0.056	0.150
	Fe ^O	16a	0.000	0.000	0.000
	Fe ^T	24d	0.375	0.000	0.250
	Gd	24c	0.125	0.000	0.250
Film under a compressive strain of -1%	O	32g	0.972	0.056	0.149
		32g	0.149	0.972	0.057
		32g	0.557	0.650	0.472
	Fe ^O	16c	0.000	0.000	0.000
	Fe ^T	16e	0.375	0.000	0.250
		8a	0.000	0.250	0.375
	Gd	16e	0.125	0.000	0.250
		8b	0.000	0.250	0.125

Hellmann-Feynman force on each atom is less than 5 meV/Å. The crystal space group of GIG bulk is identified to be $Ia\bar{3}d$ using FINDSYM [30] in our calculations, as consistent with experiments [9]. In contrast, the space group of the GIG films is $I4_1/acd$, as a result of the considered epitaxy. Our density functional calculations predict that the cubic centrosymmetric structure of GIG bulk has lattice parameters of $a = b = c = 12.405$ Å, which are in 0.5% error range of the experimental value of 12.471 Å [31], and the internal atomic positions that are shown in Table I. For comparison, Table I further shows such internal atomic positions but for a film experiencing a -1% compressive strain. The Wyckoff positions of tetrahedron Fe and Gd ions in bulk GIG are splitting into different positions under the influence of strain (such splitting gives rise to more distinct magnetic interactions in the films than in the bulk, as shown in Table II).

The exchange coupling coefficients, J , of Eq. (1) are then extracted from these DFT calculations for the bulk and any studied strain, using the four-state energy mapping method. Such latter method is detailed in Refs. [32,33]. It was previously proven to be accurate [34–38]. Practically, ten different couplings in the bulk structure, including first-nearest neighbor (1NN) and 2NN, exist within a bond length of 5.6 Å. Four of them were numerically found (when running MC simulations) to have a minimal or no influence on magnetic behavior. Therefore, we only considered the following six couplings in all our MC calculations that show noticeable influence on overall magnetic property: 1NN tetrahedron Fe (Fe^T) – octahedron Fe (Fe^O), 1NN tetrahedron Fe–Gd, 1NN tetrahedron Fe–tetrahedron Fe, 1NN octahedron Fe–Gd, 1NN octahedron Fe–octahedron Fe and 2NN tetrahedron Fe–Gd. These six interactions are listed in Table II in the bulk case, starting with the one having the largest coupling coefficient. It is also important to know that the listed 1NN J parameter between tetrahedral Fe and Gd ions has been enhanced by a 1.95 factor with respect to its DFT-extracted parameter, in order to reproduce the experimental result of T_M of Ref. [9] for the bulk system (note that we numerically found that only considering this renormalized 1NN J coefficient between tetrahedral Fe and Gd ions in our MC calculations yields an underestimation

TABLE II. Calculated renormalized exchange coupling coefficients J for the bulk GIG and (001) GIG films under a -1% compressive strain.

Coupling	Without strain J (meV)	With strain	
		-1% J (meV)	1% J (meV)
1NN Fe ^O - Fe ^T	7.456	7.852	7.244
		7.836	7.100
		7.716	7.060
1NN Fe ^T - Gd	0.808	0.958	0.836
		0.925	0.702
		0.774	0.663
1NN Fe ^T - Fe ^T	0.332	0.368	0.316
		0.352	0.304
1NN Fe ^O - Gd	-0.106	-0.103	-0.109
		-0.103	-0.106
		-0.117	-0.094
1NN Fe ^O - Fe ^O	0.096	0.096	0.092
		0.096	0.092
2NN Fe ^T - Gd	-0.063	-0.057	-0.063
		-0.054	-0.063
		-0.063	-0.069

of T_M by about 35 K but also makes the agreement with experiments for the total magnetization-*versus*-temperature curve worst, in the bulk case). Such enhancement of this parameter is also systematically used in our MC calculations for epitaxial (001) thin films. Regarding such latter films, because the structure becomes tetragonal with the $I4_1/acd$ space group, the aforementioned six different magnetic couplings of the bulk case now become 16 different couplings with different energies. Table II further shows these 16 different couplings for the films being under a compressive strain of -1% and a tensile strain of $+1\%$. These J coefficients all increase when going from tensile to compressive strains, except for the one involving a 1NN octahedron Fe-Gd interaction (this increasing tendency will be discussed in the context of altering T_M and T_C later on).

III. RESULTS

A. Magnetic properties in the bulk

We first report the results of the MC calculations for the GIG *bulk*. Figure 1(a) and its inset display the total magnetic moment and the specific heat, respectively, as a function of temperature. Figure 1(a) shows that the predicted T_M of the bulk (at which the total magnetic moment vanishes) is around 286 K, which is precisely the fitted experimental value of Ref. [9]. Moreover, a clear peak around 560 K in the specific heat can be seen, which is indicative of the magnetic phase transition from paramagnetic to ferromagnetic. Such theoretical value is consistent with the experimental result of 556 K [39]. The predicted magnetic moments also remarkably agree with the experiments of Ref. [9] for any measured temperature below 300 K, as shown in Fig. 1(a). Such agreements testify the accuracy of our calculations, once the aforementioned renormalization of a single exchange coupling parameter is accomplished. Furthermore, Fig. 1(b) shows the magnetic

moment of each individual type of magnetic ion as a function of temperature. Below the magnetic phase transition at around 560 K, spins of the Fe ions become ordered, with the overall magnetization becoming negative as a result of (i) spins of tetrahedron Fe ions being antiferromagnetically aligned with respect to spins of the octahedron Fe ions (as consistent with the strong and positive value of the J parameter of the 1NN interaction between these two types of Fe ions listed in Table II and equal to 7.456 meV) and (ii) tetrahedron and octahedron Fe ions having a 3:2 ratio in the formula unit. Furthermore, as we reach lower temperatures, the spins of the Gd ions start to become ordered and are antiparallel to those of the tetrahedron Fe ions, which is in line with the positive J parameter of 0.808 meV indicated in Table II for the 1NN Fe^T-Gd interaction. Eventually, the magnetic moment of Gd ions rises to a value that completely cancels out the overall magnetic moment of the Fe ions, which is the compensation temperature. Below such T_M , the total magnetic moment becomes positive, mostly due to the strong temperature dependency of the Gd magnetic moments. Note also that our Fig. 1(a) is qualitatively consistent with the temperature behavior of the individual magnetic moments reported for the bulk case in the Supplemental Material of Ref. [7]. On the other hand, our quantitative predictions for the Curie temperature and T_M , as well as for the temperature evolution of the total magnetic moment, are in better agreement with experiments than the data of Ref. [7] do.

Note that the residual magnetization above T_C that can be seen in the Fig. 1(a) and Fig. 1(b) is found to be related to the supercell size that is used in the MC simulations. To demonstrate that fact, we reported in Fig. 1(c) the total magnetic moment of bulk GIG as a function of temperature for different supercell sizes, that are $4 \times 4 \times 4$, $6 \times 6 \times 6$ and $8 \times 8 \times 8$. One can clearly see that there is basically no change in the magnetic moment below the Curie temperature, T_C , as the supercell size changes while the residual magnetization above T_C decreases in magnitude as the supercell size increases. Hence, in order to save computational cost, all MC calculations in this article are done on a $4 \times 4 \times 4$ supercell. Furthermore, if we analyze the J parameters in Table II, the first two couplings (1NN Fe^T-Fe^O and 1NN Fe^T-Gd) have much stronger couplings than the others, which could mean that the other magnetic couplings have negligible effect on the total magnetic moment of the system. Therefore, we show in Fig. 1(d) the total magnetic moment of bulk GIG as a function of temperature when only the two strongest magnetic couplings (mentioned above) are included. Here, the modification factor of the coupling between 1NN tetrahedron Fe-Gd ions is increased from 1.95 to 2.21, in order to match the experimental magnetization compensation temperature, T_M [9]. As a comparison, we have also included in Fig. 1(d), results where all six interactions are considered. One can see that the magnetic behavior below T_M is almost identical between these two cases, but then starts to change above T_M , which leads to different T_C . As a matter of fact, and as evidenced in the inset of Fig. 1(d), T_C increases by about 50–60 K, when only two magnetic couplings are selected with one being varied to match the experimental T_M , with respect to the T_C where all six couplings are included. The vertical dashed line in the inset reports the experimental result of

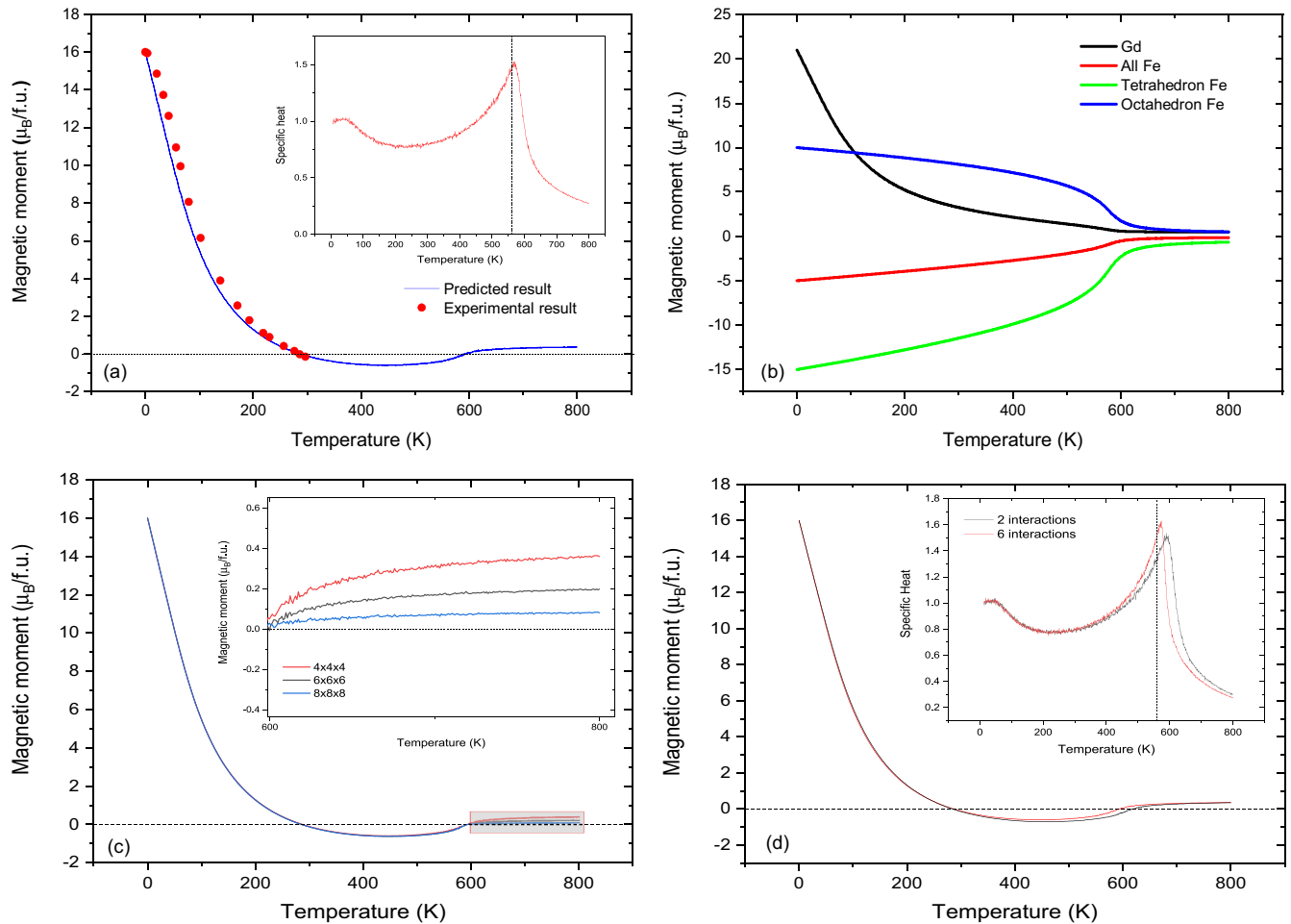


FIG. 1. Predicted total magnetic moment (a) and individual magnetic moments (b), as a function of temperature in GIG bulk. The data points in (a) show the measurements of Ref. [9]. The inset of (a) displays the temperature dependence of the specific heat (in arb. units). In this inset, the vertical line represents the experimental value of the Curie temperature [39]. (c) Predicted total magnetic moment as a function of temperature in GIG bulk for different supercells. The inset zooms in the gray area above the Curie temperature. (d) The predicted total magnetic moment as a function of temperature in GIG bulk, for which two (red color) and six (black color) magnetic interactions are considered in the calculations. The inset displays the temperature dependence of the specific heat (in arb. units) and the vertical dashed line represents the experimental value of the Curie temperature [39].

Ref. [39] for the Curie temperature and therefore attests that one needs to consider all six magnetic couplings in order to have a better agreement with observations.

B. Magnetic properties in thin films

Let us now concentrate on the epitaxial (001) GIG thin films. Under epitaxial strain (both compressive and tensile), both T_M and T_C significantly change, as revealed by the different panels of Fig. 2 and their insets. For example, a compressive strain of -3% enhances T_M from 286 to 400 K and T_C from 560 to 680 K with respect to the bulk case, while a tensile strain of $+3\%$ reduces T_M down to 193 K and T_C down to 500 K. In fact, and as shown in Fig. 3, T_M and T_C change quite linearly with respect to epitaxial strain. In particular, T_M can be varied around room temperature in the strain window ranging between -1% and $+1\%$, which is precisely the range that includes the misfit strains that should be experienced by GIG on available substrates such GGG, terbium gallium garnet (TGG), and neodymium

gallium garnet (NGG) [4]. Making T_M to be around room temperature should be highly beneficial for technologies and striking phenomena, especially when realizing that one can reverse magnetization by light around the magnetization compensation temperature [9]. Moreover, the strong effect of misfit strain on the T_C of GIG can also be of importance to have, e.g., larger magnitude of the magnetization at room temperature [see insets of Figs. 2(a) and 2(c) for compressive and tensile strains of -3% and $+3\%$]. Note also that the enhancement of T_M by applying compressive strain is reminiscent of the strengthening of the compensation temperature found in RIG systems but when applying a hydrostatic pressure [15]. However, this comparison has to be taken with a grain of salt since applying hydrostatic pressure is not similar to the application of an epitaxial strain, as, e.g., evidenced, by the fact that all three lattice parameters typically decrease under increasing hydrostatic pressure while enhancing the magnitude of epitaxial compressive strain usually results in significantly increasing the out-of-plane lattice parameter.

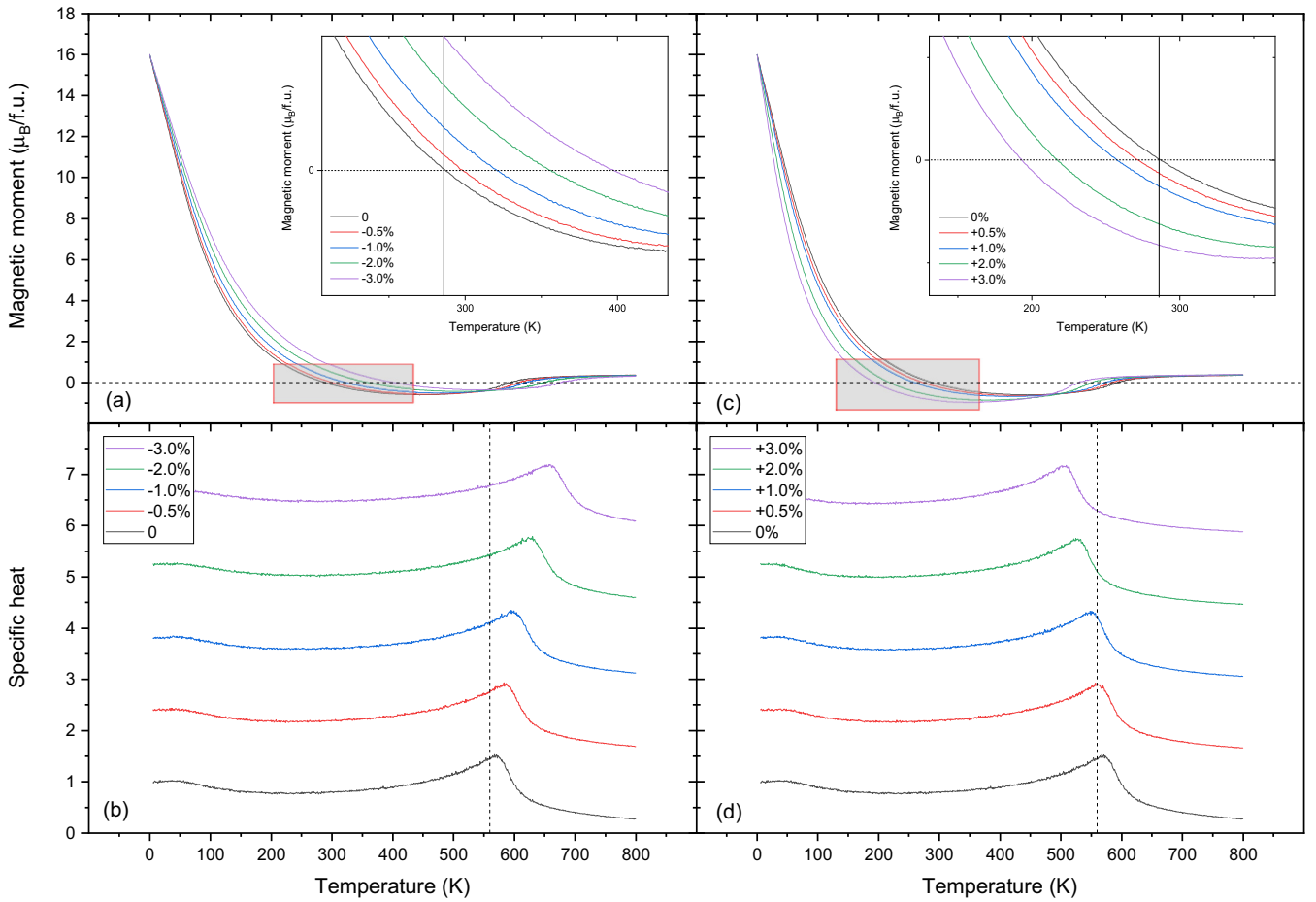


FIG. 2. Predicted magnetic properties of epitaxial (001) GIG films under different strains. (Top) Total magnetization as a function of temperature with the inset showing the magnified data of the gray box area and the vertical lines represents the experimental value of T_M [9] of GIG bulk. (Bottom) Specific heat as a function of temperature for various strains. Vertical dashed lines in these bottom figures represent the experimental value of the Curie temperature of GIG bulk [39].

We now reveal and understand the microscopic reason behind the strain-induced changes in T_C and T_M . For this, we report (i) in Figs. 4(a)–4(c) the temperature behavior of the magnitude of the individual magnetic moments of octahedron Fe, tetrahedron Fe, and Gd ions, respectively, for different strains and (ii) in Fig. 4(d) the dependence of six (average)

exchange coupling J parameters on epitaxial strain. Figures 4(a)–4(c) show that all different magnetic moments are affected by the misfit strain at any temperature. However, at higher temperatures (i.e., above about 400 K), the magnetic moments of the octahedron and tetrahedron Fe ions are the ones changing a lot under epitaxial strain while those of the Gd ions are rather small, therefore leading to the aforementioned increase in T_C when going from tensile to compressive strain. Such behaviors of the magnetic moments of the two types of Fe ions and concomitant change in T_C mostly originate for the large enhancement of the first-nearest neighbor J coupling exchanges between tetrahedral and octahedral Fe ions when going from +3% to –3%, as evidenced in Fig 4(d) and as is also consistent with Table II. On the other hand, at lower temperatures (i.e., below about 300 K), the magnetic moment of Gd is changing considerably under epitaxial strain, while the magnetic moments of these two types of Fe ions are much less sensitive to strain, as shown in Figs. 4(a)–4(c). Such difference in behaviors between the Gd and Fe ions results in the increase of T_M when varying strain from positive to negative values. It can be traced back to the fact that the magnetic moment of Gd ions is antiferromagnetically coupled with that of the tetrahedral Fe ions, and that these specific magnetic interactions has

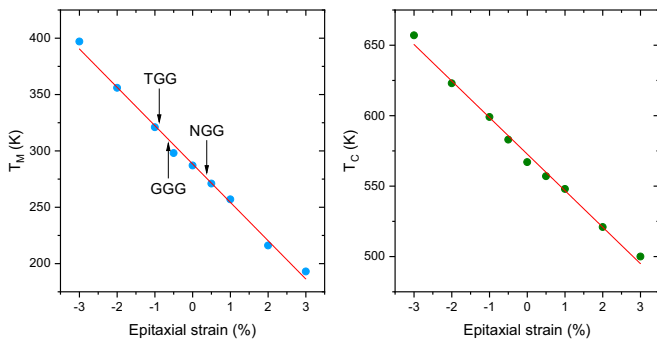


FIG. 3. Dependence of T_M (a) and T_C (b) on epitaxial strain. Misfit strains associated with possible substrates to achieve the tuning of T_M and T_C are shown in (a) by means of arrows: GGG, TGG, and NGG. The red solid lines in both panels represent linear fits of the MC data.

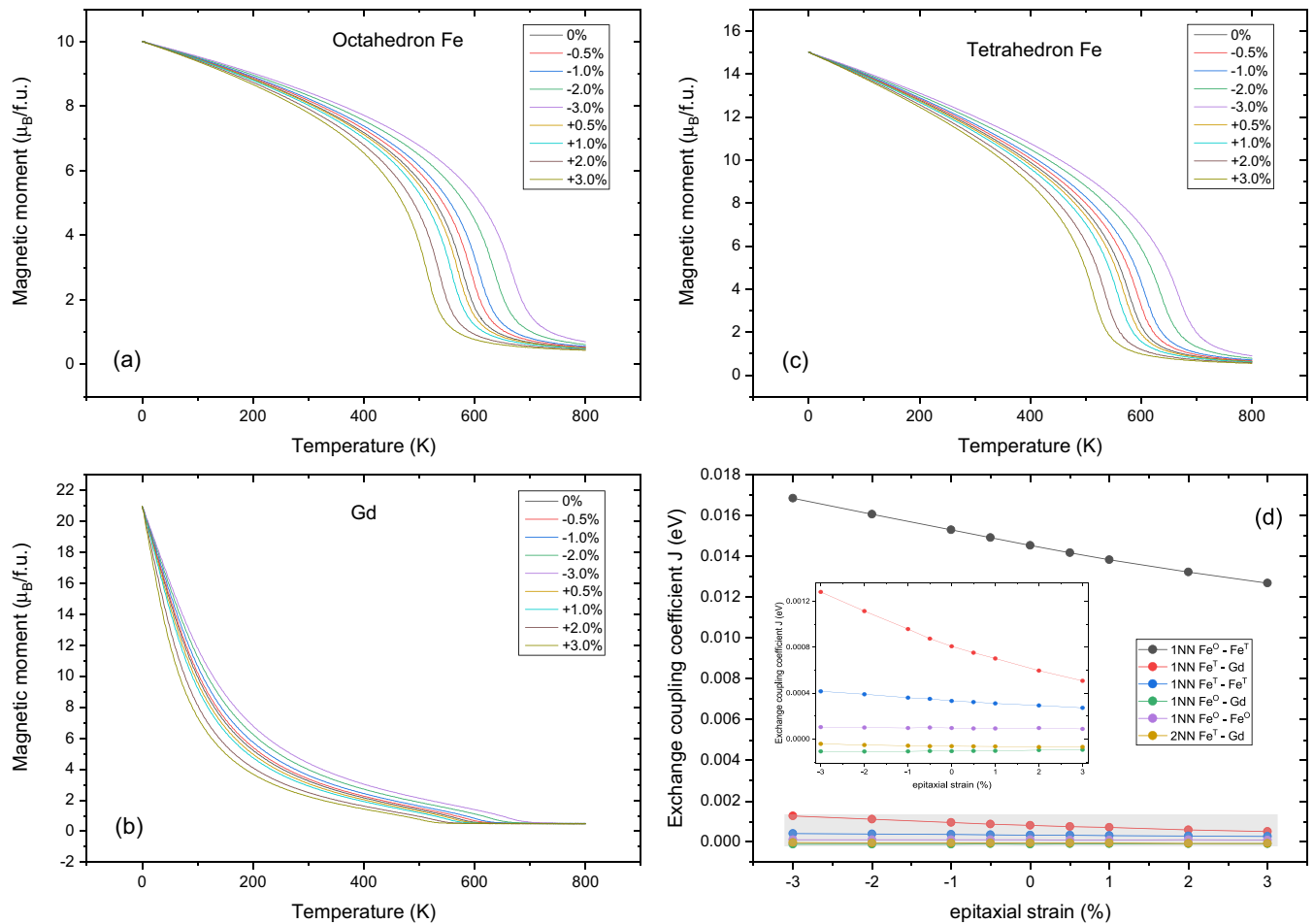


FIG. 4. Contributions from different magnetic sites to the total magnetization as a function of temperature, for different epitaxial strains (a)–(c); and dependence of exchange coupling coefficients on epitaxial strain (d). In this latter panel, each displayed exchange coupling is the *average* over similar individual parameters. For instance, three different values are averaged for the 1NN Fe^O-Fe^T interaction, as consistent with Table II.

exchange parameters that strengthen when going from +3% to −3% of strain, as revealed by Fig. 4(d) and as is consistent with Table II. One can understand such effect by realizing that compressive strain reduces the in-plane distance between the ions, resulting in an enhancement in the exchange interactions (as evidenced by the increase in the J coefficients).

IV. SUMMARY

In summary, we studied the effect of epitaxial strain on the magnetization compensation temperature and Curie temperature of the (001) GIG films via *ab initio*-based MC simulations. The changes in T_M and T_C were found to be significant and linear with the epitaxial strain, with compressive strain enhancing these two critical temperatures while the tensile strain decreases them both. The microscopic reasons behind these changes were also presently revealed, which make us believe that such strain effects should occur in *all* rare earth iron garnet systems. One can even envision the creation of a finite magnetization compensation temperature in some RIG systems that do not have T_M in their bulk form, as it seems to be, in fact, the case in some preliminary experiments done on epitaxial thulium iron garnet film [40]. Altering T_M and

T_C should bring definite advantage for spintronic applications, especially if one succeeds to bring the magnetization compensation temperature close to 300 K, as predicted here when growing (001) GIG films on the GGG substrate. It is also very likely that another critical temperature, namely the so-called angular momentum compensation temperature (which can be strongly dependent on the magnetization compensation temperature [41]), can be modified to, e.g., reach room temperature when varying the epitaxial strain in RIG films. In such a case, magnetic-field-controlled antiferromagnetic spin dynamics [42] will occur around 300 K, along with an optimization of the speed of the domain walls [43,44]. We thus hope that our results are of large benefits to the magnetic community, especially since high-quality RIG films can be nowadays grown [5,45]

ACKNOWLEDGMENTS

T.B and L.B. thank the Office of Basic Energy Sciences under Contract No. ER-46612. C.X. also thanks the Impact Grant of the Arkansas Research Alliance for financial support. D.C. acknowledges the Arkansas Department of Higher Education through the SURF grant.

- [1] K. Garello, C. O. Avci, I. M. Miron, M. Baumgartner, A. Ghosh, S. Auffret, O. Boulle, G. Gaudin, and P. Gambardella, *Appl. Phys. Lett.* **105**, 212402 (2014).
- [2] C. O. Avci, A. Quindeau, C.-F. Pai, M. Mann, L. Caretta, A. S. Tang, M. C. Onbasli, C. A. Ross, and G. S. D. Beach, *Nat. Mater.* **16**, 309 (2017).
- [3] A. V. Chumak, V. I. Vasyuchka, A. A. Serga, and B. Hillebrands, *Nat. Phys.* **11**, 453 (2015).
- [4] S. M. Zanjani and M. C. Onbasli, *AIP Adv.* **9**, 035024 (2019).
- [5] E. R. Rosenberg, L. Beran, C. O. Avci, C. Zeledon, B. Song, C. Gonzalez-Fuentes, J. Mendil, P. Gambardella, M. Veis, C. Garcia, G. S. D. Beach, and C. A. Ross, *Phys. Rev. Mater.* **2**, 094405 (2018).
- [6] K. Shen, *Phys. Rev. B* **99**, 024417 (2019).
- [7] S. Geprägs, A. Kehlberger, F. Della Coletta, Z. Qiu, E.-J. Guo, T. Schulz, C. Mix, S. Meyer, A. Kamra, M. Althammer, H. Huebl, G. Jakob, Y. Ohnuma, H. Adachi, J. Barker, S. Maekawa, G. E. W. Bauer, E. Saitoh, R. Gross, S. T. B. Goennenwein, and M. Kläui, *Nat. Commun.* **7**, 10452 (2016).
- [8] R. Nakamoto, B. Xu, C. Xu, H. Xu, and L. Bellaiche, *Phys. Rev. B* **95**, 024434 (2017).
- [9] S. Geller, J. P. Remeika, R. C. Sherwood, H. J. Williams, and G. P. Espinosa, *Phys. Rev.* **137**, A1034 (1965).
- [10] A. I. Popov, Z. V. Gareeva, and A. K. Zvezdin, *Phys. Rev. B* **92**, 144420 (2015).
- [11] M. Deb, P. Molho, B. Barbara, and J.-Y. Bigot, *Phys. Rev. B* **97**, 134419 (2018).
- [12] E. Sawatzky and E. Kay, *J. Appl. Phys.* **40**, 1460 (1969).
- [13] E. Sawatzky and E. Kay, *J. Appl. Phys.* **42**, 367 (1971).
- [14] M. Oron, I. Barlow, and W. F. Traber, *J. Mater. Sci.* **4**, 271 (1969).
- [15] D. Bloch, F. Chassé, and R. Pauthenet, *J. Appl. Phys.* **38**, 1029 (1967).
- [16] W. Haubenreisser, *Krist. Tech.* **14**, 1490 (1979).
- [17] H. Adachi and H. Ino, *Nature (London)* **401**, 148 (1999).
- [18] Y. Cao, S. Cao, W. Ren, Z. Feng, S. Yuan, B. Kang, B. Lu, and J. Zhang, *Appl. Phys. Lett.* **104**, 232405 (2014).
- [19] H. J. Zhao, J. Íñiguez, X. M. Chen, and L. Bellaiche, *Phys. Rev. B* **93**, 014417 (2016).
- [20] K. J. Choi, M. Biegalski, Y. L. Li, A. Sharan, J. Schubert, R. Uecker, P. Reiche, Y. B. Chen, X. Q. Pan, V. Gopalan, L.-Q. Chen, D. G. Schlom, and C. B. Eom, *Science* **306**, 1005 (2004).
- [21] O. Diéguez, S. Tinte, A. Antons, C. Bungaro, J. B. Neaton, K. M. Rabe, and D. Vanderbilt, *Phys. Rev. B* **69**, 212101 (2004).
- [22] N. A. Pertsev, A. G. Zembilgotov, and A. K. Tagantsev, *Phys. Rev. Lett.* **80**, 1988 (1998).
- [23] P. Sellappan, C. Tang, J. Shi, and J. E. Garay, *Mater. Res. Lett.* **5**, 41 (2017).
- [24] Y. Miyatake, M. Yamamoto, J. J. Kim, M. Toyonaga, and O. Nagai, *J. Phys. C* **19**, 2539 (1986).
- [25] G. Kresse and D. Joubert, *Phys. Rev. B* **59**, 1758 (1999).
- [26] P. E. Blöchl, *Phys. Rev. B* **50**, 17953 (1994).
- [27] J. P. Perdew, A. Ruzsinszky, G. I. Csonka, O. A. Vydrov, G. E. Scuseria, L. A. Constantin, X. Zhou, and K. Burke, *Phys. Rev. Lett.* **100**, 136406 (2008).
- [28] O. Diéguez, O. E. González-Vázquez, J. C. Wojdeł, and J. Íñiguez, *Phys. Rev. B* **83**, 094105 (2011).
- [29] C. Xu, Y. Yang, S. Wang, W. Duan, B. Gu, and L. Bellaiche, *Phys. Rev. B* **89**, 205122 (2014).
- [30] H. T. Stokes and D. M. Hatch, *J. Appl. Crystallogr.* **38**, 237 (2005).
- [31] G. P. Espinosa, *J. Chem. Phys.* **37**, 2344 (1962).
- [32] H. J. Xiang, E. J. Kan, S.-H. Wei, M.-H. Whangbo, and X. G. Gong, *Phys. Rev. B* **84**, 224429 (2011).
- [33] H. Xiang, C. Lee, H.-J. Koo, X. Gong, and M.-H. Whangbo, *Dalton Trans.* **42**, 823 (2013).
- [34] X. Z. Lu, M.-H. Whangbo, S. Dong, X. G. Gong, and H. J. Xiang, *Phys. Rev. Lett.* **108**, 187204 (2012).
- [35] C. Gong, L. Li, Z. Li, H. Ji, A. Stern, Y. Xia, T. Cao, W. Bao, C. Wang, Y. Wang, Z. Q. Qiu, R. J. Cava, S. G. Louie, J. Xia, and X. Zhang, *Nature (London)* **546**, 265 (2017).
- [36] C. Xu, J. Feng, H. Xiang, and L. Bellaiche, *Npj Comput. Mater.* **4**, 57 (2018).
- [37] Y. Deng, Y. Yu, Y. Song, J. Zhang, N. Z. Wang, Z. Sun, Y. Yi, Y. Z. Wu, S. Wu, J. Zhu, J. Wang, X. H. Chen, and Y. Zhang, *Nature (London)* **563**, 94 (2018).
- [38] C. Xu, B. Xu, B. Dupé, and L. Bellaiche, *Phys. Rev. B* **99**, 104420 (2019).
- [39] K. P. Belov, E. V. Talalaeva, and G. A. Yarkho, *Sov. Phys. JETP* **25**, 989 (1967).
- [40] Y. Ma and C. Cen, APS March Meet. 2019, Abstr. Id.R40.013 (2019).
- [41] Y. Hirata, D.-H. Kim, T. Okuno, T. Nishimura, D.-Y. Kim, Y. Futakawa, H. Yoshikawa, A. Tsukamoto, K.-J. Kim, S.-B. Choe, and T. Ono, *Phys. Rev. B* **97**, 220403(R) (2018).
- [42] K.-J. Kim, S. K. Kim, Y. Hirata, S.-H. Oh, T. Tono, D.-H. Kim, T. Okuno, W. S. Ham, S. Kim, G. Go, Y. Tserkovnyak, A. Tsukamoto, T. Moriyama, K.-J. Lee, and T. Ono, *Nat. Mater.* **16**, 1187 (2017).
- [43] L. Caretta, M. Mann, F. Büttner, K. Ueda, B. Pfau, C. M. Günther, P. Helsing, A. Churikova, C. Klose, M. Schneider, D. Engel, C. Marcus, D. Bono, K. Bagschik, S. Eisebitt, and G. S. D. Beach, *Nat. Nanotechnol.* **13**, 1154 (2018).
- [44] S. A. Siddiqui, J. Han, J. T. Finley, C. A. Ross, and L. Liu, *Phys. Rev. Lett.* **121**, 057701 (2018).
- [45] C. N. Wu, C. C. Tseng, Y. T. Fanchiang, C. K. Cheng, K. Y. Lin, S. L. Yeh, S. R. Yang, C. T. Wu, T. Liu, M. Wu, M. Hong, and J. Kwo, *Sci. Rep.* **8**, 11087 (2018).